THE JOURNAL OF PHYSICAL CHEMISTRY B
A JOURNAL OF THE AMERICAN CHEMICAL SOCIETY

pubs.acs.org/JPCB

Article

New Two-Photon Absorbing Squaraine Derivative with Efficient Near-Infrared Fluorescence, Superluminescence, and High Photostability

Mykhailo V. Bondar,* Sanaz Faryadras, Natalia Munera, Hao-Jung Chang, Mehrun Uddin, Kevin D. Belfield, Olexiy D. Kachkovsky, Eric W. Van Stryland, and David J. Hagan*

Cite This: *J. Phys. Chem. B* 2022, 126, 3897−3907

Read Online

ACCESS | Metrics & More | Article Recommendations

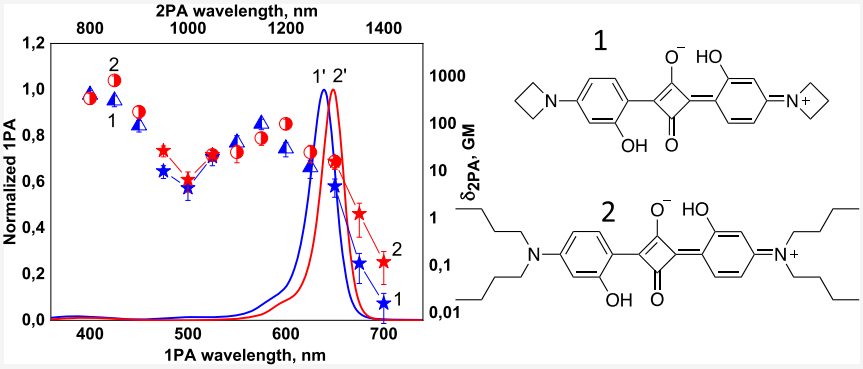

ABSTRACT: The nature of linear photophysical and nonlinear optical properties of a new squaraine derivative 2,4-bis[4-(azetidyl)-2-hydroxyphenyl]squaraine (**1**) with efficient near-infrared (NIR) emission was comprehensively analyzed based on spectroscopic, photochemical, and two-photon absorption (2PA) measurements, along with quantum chemical analysis. The steady-state absorption, fluorescence, and excitation anisotropy spectra of **1** and its fluorescence emission lifetimes revealed the multiple aspects of the electronic structure of **1**, including the relative orientations of the main transition dipoles, effective rotational volumes in solvents of different polarities, and a maximum molar extinction of 1.35×10^{-5} $M^{-1}{\cdot}cm^{-1}$, which is unusually small for similar symmetric squaraines. The degenerate 2PA spectrum of **1** was obtained over a broad spectral range under femtosecond excitation, using standard open-aperture Z-scan and two-photon induced fluorescence methods, revealing maximum 2PA cross sections of ∼400 GM. Squaraine **1** exhibited efficient superluminescence emission in the polar solvent (dichloromethane) at room temperature under femtosecond pumping conditions. Quantum chemical analysis of the electronic structure of **1** was performed using the DFT/TD-DFT level of theory and found to be in good agreement with experimental data. The new squaraine derivative **1** displayed high fluorescence quantum yield, efficient NIR superluminescence, large 2PA cross sections, and high photostability with a photodecomposition quantum yield $\sim 4 \times 10^{-6}$, suggesting its potential for applications in two-photon fluorescent bioimaging and lasing.

1. INTRODUCTION

The development of new squaraine derivatives with intense linear absorption bands, efficient near-infrared (NIR) emission, large two-photon absorption (2PA) cross sections, and high photostability is a subject of interest for a number of important scientific and technological areas, including nonlinear optics,[1] optical data recording,[2] optoelectronics,[3−5] metal-ion sensing,[6] photodynamic therapy,[7,8] and fluorescence bioimaging,[9−11] among others. In general, squaraine derivatives can be presented as resonantly stabilized zwitterionic structures[8,12,13] with an electron-deficient central squarainyl ring C_4O_2 and electron-donating termini.[14−16] Certain squaraine molecules exhibit high photochemical stability[17−19] and possess a wide variety of specific linear and nonlinear spectroscopic properties determined by the specific structure of the molecular architecture, including intramolecular steric factors,[4,20,21] hydrogen bonding,[22] symmetry of the electronic distribution,[19,23,24] and parameters of the terminal groups.[13,16,25−27]

Received: February 22, 2022
Revised: April 30, 2022
Published: May 18, 2022

https://doi.org/10.1021/acs.jpcb.2c01288
J. Phys. Chem. B 2022, 126, 3897−3907

The majority of symmetrical squaraine derivatives (with corresponding quadrupolar molecular structure: donor−acceptor−donor[15,28]) are characterized by relatively sharp, intense long-wavelength absorption bands in the red-NIR spectral range (maximum extinction coefficient, $\varepsilon^{max} \sim (3-4) \times 10^5$ M^{-1} cm^{-1}),[18,29,30] high fluorescence quantum yields, $\Phi_{fl} > 0.6$,[18,31,32] and some of the highest single-molecule 2PA efficiencies (corresponding 2PA cross sections, $\delta_{2PA}^{max} \sim 10^4$ GM).[11,33−35] The nature of these large values of δ_{2PA}^{max} for symmetrical squaraines is mainly determined by the large ε^{max} and the possibility to realize double-resonance excitation conditions.[35] Squaraine derivatives with unsymmetrical molecular structures often exhibit much broader absorption bands with smaller values of ε^{max}[36] and possess significant potential for applications in organic solar cell engineering.[5,23,37]

All types of squaraine molecules typically reveal a strong decrease in emission intensity with the increase in polarity of the surrounding medium[20,26,30−33,38] that can be explained by the increased efficiency of the nonradiative vibronic relaxations, which dramatically reduce their fluorescence. In this study, we present the synthesis and comprehensive characterization of this new 2,4-bis[4-(azetidyl)-2-hydroxyphenyl]squaraine (**1**) with potential for two-photon fluorescence microscopy applications.[9,11,17] Linear photophysical, photochemical, 2PA, and superluminescence properties of **1** were investigated in comparison with a known analogous squaraine structure 2,4-bis [4-(N,N-dibutylamino)-2-hydroxyphenyl]squaraine[39] (**2**) in liquid media at room temperature (see structures in Figure 1). The electronic

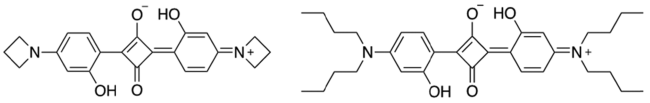

Figure 1. Molecular structure of squaraine dyes.

properties of **1** and **2** were also analyzed with density functional theory (DFT)/time-dependent DFT (TD-DFT) quantum-chemical calculations, and the essential excited states, oscillator strengths of the corresponding electronic transitions, main molecular orbital configurations, and the role of the end substituents are described.

2. EXPERIMENTAL SECTION

2.1. Synthesis of Azetidyl-Functionalized and Reference Squaraines. The azetidyl starting material and reference squaraine **2** were prepared using previously reported methods,[40,41] and the ^{1}H and ^{13}C NMR results were consistent with the reported data. The main synthetic procedures for **1** and **2** are presented in Schemes 1 and 2, respectively.

*2.1.1. Synthesis of 2,4-bis[4-(azetidyl)-2-hydroxyphenyl]-squaraine (**1**).* 3-(Azetid-1-yl)phenol was prepared using a previously reported method.[40] A round-bottom flask was charged with $Pd(OAc)_2$ (0.579 mmol) in toluene (30 mL) and backfilled with nitrogen. Sequentially, 3-bromophenol (11.6 mmol), 2,8,9-triisobutyl-2,5,8,9-tetraaza-1-phosphabicyclo[3.3.3]undecane ("Verkade base", 1.16 mmol), and LiHMDS (1.0 M in THF, 26.6 mmol) were added to the flask, after which azetidine (13.9 mmol) was added slowly, and the reactants was stirred at 80 °C for 18 h. The mixture was cooled to room temperature, deposited onto silica, and washed with hexane and ethyl acetate. The solvent was removed under pressure and purified by silica gel chromatography (70:30, hexanes:ethyl acetate). ^{1}H NMR of 3-(azetid-1-yl)phenol (500 MHz, $CDCl_3$) δ: 7.04 (t, 1H), 6.19 (ddd, 1H), 6.05 (ddd, 1H), 5.92 (t, 1H), 4.77 (s, 1H), 3.85 (t, 4H), 2.35 ppm (p, 2H). ^{13}C NMR of 3-(azetid-1-yl)phenol (500 MHz, $CDCl_3$) δ: 156.48, 153.78, 129.94, 104.54, 104.27, 98.49, 52.40, 16.86 ppm.

The final product **1** was prepared by charging a round-bottom flask, fitted with a Dean−Stark apparatus, with squaric acid (1 mol) in a 1-butanol (15 mL) and toluene (6 mL) mixture. The solution was heated to 100 °C for 15 min to allow the squaric acid to dissolve. Subsequently, 3-(azetid-1-yl)phenol (2 mol) in toluene (8 mL) was added dropwise over 20 min. The solution was heated to reflux for 2 h. Blue solid was obtained through filtration and washed with ethyl acetate. The product was extracted from the solid by washing with chloroform. ^{1}H NMR of **1** (500 MHz, $CDCl_3$) δ: 12.17 (s, 2H), 7.89 (d, 2H), 5.99 (dd, 2H), 5.77 (d, 2H), 4.15 (t, 8H), 2.48 ppm (quintet, 4H). HR-MS (ESI) (m/z): [M + H] + Calculated for $C_{22}H_{21}N_2O_4$, 377.1496; Found, 377.1492.

*2.1.2. Synthesis of 2,4-bis [4-(N,N-dibutylamino)-2-hydroxyphenyl]squaraine (**2**).* A round-bottom flask, fitted with a Dean−Stark apparatus, was charged with squaric acid (1 mol) in a 1-butanol (15 mL) and toluene (6 mL) mixture. The solution was heated to 100 °C for 15 min to allow the squaric acid to dissolve. Subsequently, N,N-(dibutylamino)phenol (2 mol) in toluene (8 mL) was added dropwise over 20 min. The solution was heated to reflux for 2 h. Green crystals were obtained through filtration and washed with ethyl acetate. ^{1}H NMR of **2** (500 MHz, $CDCl_3$) δ: 12.15 (s, 2H), 7.92 (d, 2H), 6.37 (dd, 2H), 6.17 (d, 2H), 3.43 (t, 8H), 1.68 (quintet, 8H), 1.44 (sextet, 8H), 1.03 ppm (t, 12H). ^{13}C NMR of **2** (500 MHz, $CDCl_3$) δ: 183.07, 172.17, 164.13, 156.40132.85, 109.83, 107.61, 98.53, 51.41, 29.85, 20.26, 13.93 ppm.

2.2. Linear Photophysical and Photochemical Characterization of 1 and 2. All linear photophysical and photochemical measurements were performed in air-saturated spectroscopic-grade dichloromethane (DCM) and toluene (TOL), which were purchased from commercial sources and used without further purification. The steady-state linear or one-photon absorption (1PA) spectra of **1** and **2** were recorded with a high-performance Cary 5000 UV−vis−NIR (Agilent) spectrophotometer using 1 cm path length quartz cuvettes and squaraine concentrations, C ≈ (3−5) × 10^{-6} M. The steady-state and time-resolved fluorescence measure-

Scheme 1. Synthetic Route for Azetidyl-Functionalized Squaraine 1

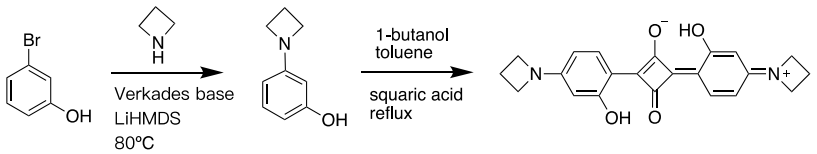

https://doi.org/10.1021/acs.jpcb.2c01288
J. Phys. Chem. B 2022, 126, 3897−3907

Scheme 2. Synthetic Route for Reference Squaraine 2

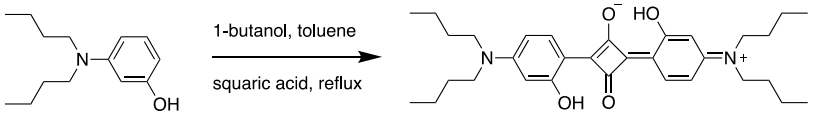

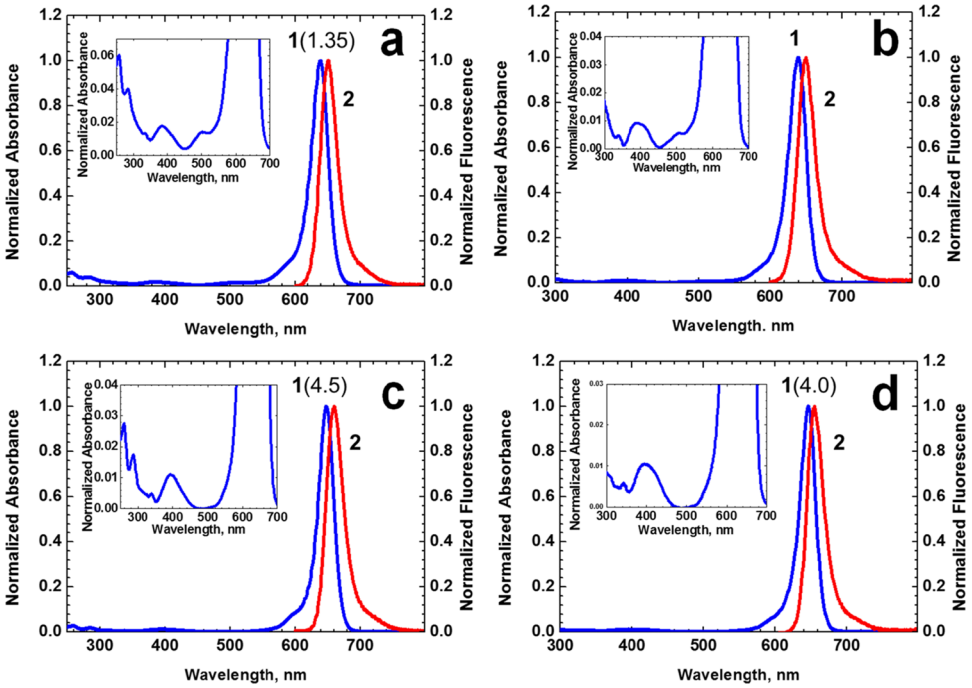

Figure 2. Normalized steady-state 1PA (1) and fluorescence (2) spectra of **1** in DCM (a), TOL (b), **2** in DCM (c), and TOL (d). Number in the parentheses represents the maximum extinction coefficient ($\varepsilon^{max} \times 10^{-5}$, $M^{-1}\cdot cm^{-1}$).

ments, including corrected fluorescence and excitation anisotropy spectra values of the fluorescence quantum yields, Φ_{fl}, and emission lifetimes, τ_{fl}, were determined using a FLS980 spectrofluorimeter (Edinburg Instruments Ltd.) with dilute solutions ($C \approx (1-2) \times 10^{-7}$ M) and standard spectrofluorimetric quartz cuvettes. Fluorescence quantum yields of **1** and **2** were determined using a standard comparative method[42] with cresyl violet in methanol as a reference ($\Phi_{fl} \approx 0.54$).[43]

The fundamental excitation anisotropy spectra, $r_0(\lambda)$, for **1** and **2** were obtained at room temperature in viscous polytetrahydrofuran (pTHF), where the molecular rotational correlation time, $\theta = \eta \cdot V/kT$ (η, V, k, and T are the solvent viscosity, effective rotational volume of the molecule, Boltzmann constant, and absolute temperature, correspondingly)[44] was much larger than τ_{fl} and rotational depolarization effects were negligible. In this case, the experimentally observed excitation anisotropy spectrum $r(\lambda) = r_0(\lambda)/(1 + \tau_{fl}/\theta) \approx r_0(\lambda)$.[42] Photochemical stabilities of **1** and **2** were investigated in air-saturated TOL and DCM under continuous wave (CW) laser irradiation at $\lambda = 637$ nm with average beam irradiance ≈ 500 mW/cm^2. Corresponding values of the photodecomposition quantum yields, Φ_{ph} (i.e., the number of decomposed molecules divided by the number of absorbed photons), were determined by a known absorption method[45] as

$$\Phi_{ph} = \frac{[D(\lambda, 0) - D(\lambda, t_{ir})]\cdot N_A}{\varepsilon(\lambda)\cdot 10^3 \cdot \int_\lambda \int_0^{t_{ir}} I_0(\lambda)\cdot[1 - 10^{-D(\lambda,t)}]\cdot d\lambda\cdot dt} \quad (1)$$

where $D(\lambda,0)$, $D(\lambda, t_{ir})$, $\varepsilon(\lambda)$, N_A, λ, t_{ir}, and $I_0(\lambda)$ are the values of initial and final absorbance of the sample solution, extinction coefficient (in $M^{-1}\cdot cm^{-1}$), Avogadro's number, excitation wavelength, irradiation time, and spectral distribution of the excitation irradiance, respectively.

2.3. 2PA Spectra and Superluminescence Measurements. Nonlinear optical properties of **1** and **2** were investigated in DCM at room temperature using femtosecond laser systems and corresponding experimental techniques, described in detail previously.[17,19,46] The degenerate 2PA spectra were obtained over a broad spectral range (800−1400 nm) by open-aperture Z-Scan[47] and two-photon-induced fluorescence (2PF) methods[48] using 1 and 10 mm path length quartz cuvettes with dye concentrations $C \sim 10^{-3}$ and $C \sim 10^{-5}$ M, respectively. The exit beam from the optical parametric amplifier (OPA, TOPAS C, Light Conversion Ltd., with pulse energy, $E_P \leq 250$ μJ, pulse duration, $\tau_P \approx 150$ fs, and repetition rate 1 kHz), which was pumped by the regenerative amplifier (Clark MXR, CPA 2010), was employed for Z-scan measurements. The same laser beam in combination with the PTI spectrofluorimeter was used for 2PF measurements. The superluminescence of **1** and **2** was observed from the 10 mm spectrofluorimetric quartz cuvettes with dye concentrations $\sim 10^{-4}$ M under femtosecond pumping by the second harmonic of the OPA tuned to 1300 nm. The pump laser beam (excitation wavelength, $\lambda_{exc} \approx 650$ nm, $E_P \leq 5$ μJ)

https://doi.org/10.1021/acs.jpcb.2c01288
J. Phys. Chem. B 2022, 126, 3897−3907

Table 1. Linear Spectroscopic and Photochemical Parameters of New Squaraine 1 and Reference One 2 in TOL and DCM[a]

compound	1		2	
solvent	TOL	DCM	TOL	DCM
λ_{ab}^{max}, nm	639 ± 1	639 ± 1	646 ± 1	648 ± 1
λ_{fl}^{max}, nm	650 ± 1	651 ± 1	654 ± 1	660 ± 1
Stokes shift, nm (cm^{-1})	11 ± 2 (260 ± 30)	12 ± 2 (290 ± 30)	8 ± 2 (190 ± 20)	12 ± 2 (280 ± 20)
$\varepsilon^{max} \times 10^{-5}$, $M^{-1}\cdot cm^{-1}$		1.35 ± 0.15	4.5 ± 0.3	4.0 ± 0.2
μ_{01}, Debye		8.8	14.2	14.0
Φ_{fl}	0.97 ± 0.05	0.77 ± 0.05	0.88 ± 0.05	0.86 ± 0.05
τ_{fl}, ns	2.5 ± 0.2	2.6 ± 0.2	2.5 ± 0.1	2.6 ± 0.2
τ_{fl}^{cal}, ns		4.8 ± 1	1.6 ± 0.3	2.1 ± 0.4
$r(\lambda_{ab}^{max})$	0.016 ± 0.003	0.015 ± 0.003	0.026 ± 0.005	0.020 ± 0.004
θ, ns	0.15 ± 0.05	0.14 ± 0.04	0.21 ± 0.06	0.17 ± 0.05
V, Å^3	1050	1450	1470	1760
$\Phi_{ph} \times 10^6$		3.8 ± 0.8	0.02 ± 0.004	1.4 ± 0.3

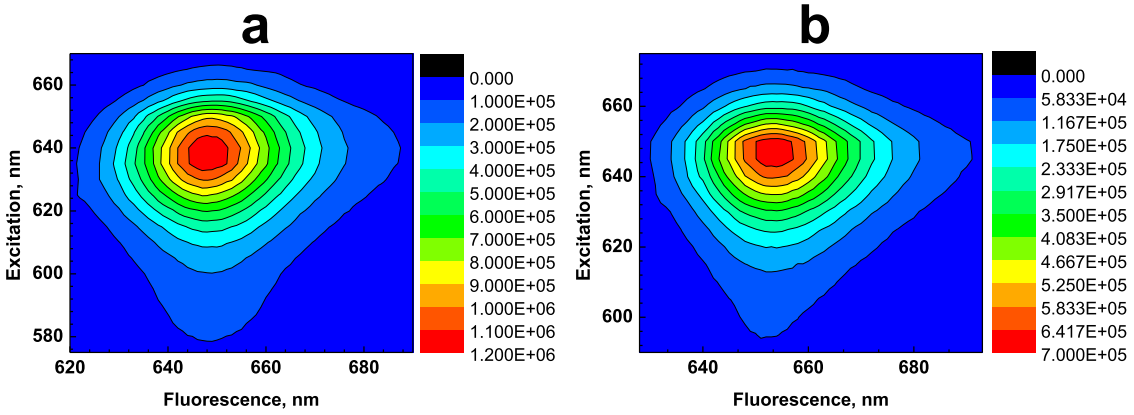

Figure 3. 3D fluorescence emission maps of 1 (a) and 2 (b) in TOL.

was focused by a cylindrical lens to a waist of 0.15 × 10 mm while superluminescence emission was detected in the transverse direction by a fiber optic spectrometer (HR4000, Ocean Optics, Inc.).

2.4. Computational Analysis. The nature of the electronic properties of **1** and **2** was estimated by quantum-chemical calculations, which were performed with the Gaussian 2009, Rev.A02.[49] DFT with the 6-31G(d,p) basis set and the B3LYP functional was used for geometry optimization. TD-DFT was employed to describe the excited state (including the optimized geometry). The polarizable continuum model (PCM)[50] has been used to take into account the surrounding solvent. Based on the known negligible effect of alkyl substituents on the electronic properties of symmetrical squaraines,[51] the *n*-butyl groups on the nitrogens in model compound **2** were replaced by methyl groups. All linear spectral parameters were predicted using optimized ground and first excited singlet electronic-state molecular geometry for absorption and emission spectra, respectively.

3. RESULTS AND DISCUSSION

3.1. Linear Spectral and Photochemical Properties of 1 and 2. The main photophysical characteristics and photodecomposition quantum yields, Φ_{ph}, of the new squaraine derivative **1** and reference compound **2** are presented in Figure 2 and Table 1. The linear 1PA spectra of **1** and **2** exhibit relatively sharp (FWHM ~30 nm) and intense ($\varepsilon^{max} > 1.3 \cdot 10^5$ M^{-1} cm^{-1}) long-wavelength absorption bands with maxima at ~640−680 nm (Figure 2, curves 1), which are typical for symmetrical squaraines in this spectral range.[15,18,20] Very weak short-wavelength linear absorption bands at ~400 nm were observed for **1** and **2** in both solvents studied (see insets in Figure 2), which potentially can be active in 2PA processes.[15,35] It should be mentioned that a large difference in the values of ε^{max} was obtained for **1** and **2** in DCM (Table 1 showing ε^{max} (**1**) < ε^{max} (**2**)), which is not clearly understood because of the similarity of the molecular structures and all other linear photophysical parameters determined in this work. The solubility of **1** in TOL was relatively low compared to **1** and **2** in DCM while no evidence of aggregation was observed. Hence, these processes cannot be a reason for the large difference in ε^{max}. Fluorescence emission spectra of squaraine **1** were similar to those of reference compound **2** in TOL and DCM with small Stokes shifts (<15 nm) and full independence of the excitation wavelength (i.e., without violation of Kasha's rule[42]). Three-dimensional (3D) fluorescence maps for **1** and **2** (Figure 3) confirm this assertion along with the full independence of the corresponding excitation spectra of the observed wavelength. The fluorescence emission quantum yields, Φ_{fl}, were relatively high (see Table 1), especially for **1** in TOL ($\Phi_{fl} \approx 1.0$), which can be employed as a fluorescence reference standard in the red-NIR spectral range. The kinetics of fluorescence decay of **1** and **2** was characterized by a single-exponential process in TOL and DCM (Figure 4) with the characteristic lifetimes $\tau_{fl} \approx 2.5-2.6$ ns, which were nearly the same for both squaraines and does not explain the nature of such a large difference in their ε^{max} and corresponding transition dipoles,

https://doi.org/10.1021/acs.jpcb.2c01288
J. Phys. Chem. B 2022, 126, 3897−3907

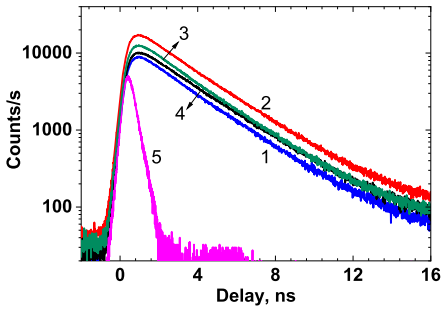

Figure 4. Kinetics of fluorescence decay for squaraine **1** (1, 2) and **2** (3, 4) in TOL (1, 3) and DCM (2, 4), and instrument response function (5).

$\mu_{01} \approx 0.096 \cdot \sqrt{\int \varepsilon(\nu) \cdot \lambda_{ab}^{max} \cdot d\nu}$, estimated from the experimental data (μ_{01} in Debye, extinction coefficient in the main absorption band, $\varepsilon(\nu)$ in $M^{-1} \cdot cm^{-1}$, λ in cm, and ν in cm^{-1}).[52]

[a]Steady-state absorption λ_{ab}^{max} and fluorescence λ_{fl}^{max} maxima; values of Stokes shifts; maximum extinction coefficients, ε^{max}; fluorescence emission quantum yields, Φ_{fl}; estimated transition dipoles for $S_0 \rightarrow S_1$ electronic transition, μ_{01} (S_0 and S_1 are the ground and first excited electronic state, correspondingly);[52] experimentally observed, τ_{fl}, and calculated, τ_{fl}^{cal}, fluorescence lifetimes;[53] excitation anisotropies, $r(\lambda_{ab}^{max})$, rotational correlation times, θ, effective rotational volume, V, and photodecomposition quantum yields, Φ_{ph}.

Experimentally observed fluorescence lifetimes τ_{fl} can be also calculated from the linear spectral data of **1** and **2** as[42] $\tau_{fl}^{cal} = \tau_N \cdot \Phi_{fl}$, where τ_N is the natural lifetime that can be determined from the Strickler–Berg theoretical approach.[53] The values of τ_{fl}^{cal} are in a good agreement with experimental ones for reference squaraine **2** (see Table 1), which is evidence of relatively small changes in the molecular geometry under electronic excitation $S_0 \rightarrow S_1$ and fulfillment of the mirror symmetry between absorption and emission contours.[54] In contrast, a large discrepancy was observed for the corresponding lifetimes for **1**, which can be related to an unusually small (for symmetrical squaraines) value of ε^{max}. The steady-state fundamental excitation anisotropy spectra of **1** and **2**, $r_0(\lambda)$, were obtained in viscous pTHF (Figure 5, curves 1) that reveal the nature of the main 1PA band: nearly constant values of $r_0(\lambda) \approx$ const in the spectral range ≈ 560–670 nm are related to the dominant role of a single electronic transition $S_0 \rightarrow S_1$ in the main long-wavelength absorption band of **1** and **2**.[55] The maxima values of $r_0(\lambda) \approx 0.3$ provide an estimation of the angle between the absorption, $\boldsymbol{\mu}_{01}$, and emission, $\boldsymbol{\mu}_{10}$, transition dipoles as ≈25°, which is too large to allow for a correct determination of the relative orientations of the corresponding absorption dipoles $\boldsymbol{\mu}_{01}$ and $\boldsymbol{\mu}_{0n}$ (n is the number of higher excited electronic state).[55] Excitation anisotropy spectra $r(\lambda)$ were also determined for **1** and **2** in low-viscosity TOL and DCM (Figure 5, curves 2, 3) in order to determine $r(\lambda_{ab}^{max})$, rotational correlation times, θ, and effective rotational volume, V (see Section 2.2 and Table 1). It should be noted that within the main absorption band, the signal to noise in the low-viscosity solvents is significant. According to these data, the values of θ exhibit a relatively weak dependence on solvent polarity in contrast to the effective rotational volumes, V, which exhibit a noticeable increase in the size of the solvate cage in more polar solvents for both of the investigated squaraines.

The level of the photochemical stability of **1** and **2** was investigated quantitatively in air-saturated TOL and DCM at room temperature using the absorption method[45] with low-intensity laser irradiation in the main absorption band at $\lambda \approx$ 637 nm. Accordingly, small changes in the main absorption bands of **1** and **2** (Figure 6) were detected during the irradiation process, and the corresponding values of the photodecomposition quantum yields, Φ_{ph}, were calculated by eq 1 and shown in Table 1. It should be mentioned that the kinetics of the observed photodecomposition processes corresponded to a first-order photoreaction,[56] and no substantial photoproducts were detected near the 1PA maxima of **1** and **2**. From these data, the highest photostability was observed for **2** in TOL ($\Phi_{ph} \sim 10^{-8}$) and dramatically decreased up to two orders of magnitude in polar DCM. The level of photostability of new squaraine **1** is somewhat lower than that of **2** but still comparable with the best laser dyes in liquid media[57] and can be used for important practical applications, including as a contrast agent in laser scanning fluorescence microscopy techniques.[9]

3.2. 2PA Properties and Superluminescence Effects in Liquid Solutions of 1 and 2. The values of 2PA cross sections, δ_{2PA}^{max}, were obtained for **1** and **2** in DCM using direct open-aperture Z-Scan[47] and relative 2PF[48] methods, while the corresponding degenerate spectra are shown in Figure 7. As follows from these data, the shape of the obtained 2PA spectra is similar to some known symmetric squaraines[18,32,34] with the weak maximum ($\delta_{2PA}^{max} \approx$ 90–100 GM) at ~1150 to 1200 nm and strong increase (up to 400–830 GM) in the short-wavelength spectral range at ~800–850 nm. It is worth noting

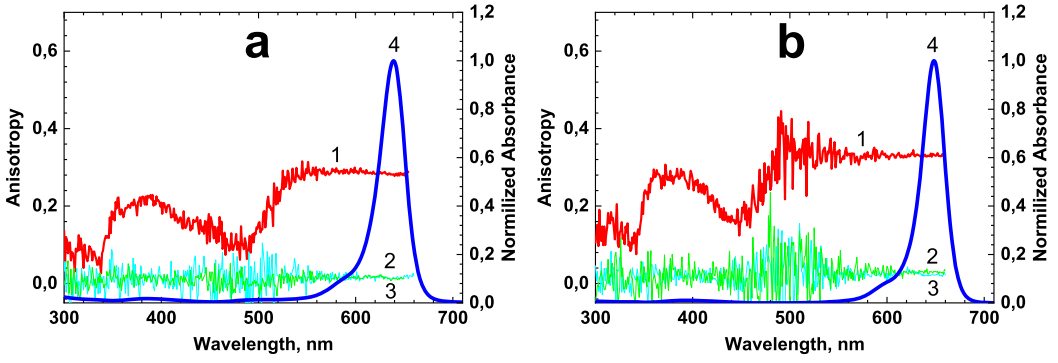

Figure 5. Steady-state excitation anisotropy spectra of squaraine **1** (a) and **2** (b) in pTHF (1), TOL (2), and DCM (3); corresponding linear 1PA spectra in DCM (4).

https://doi.org/10.1021/acs.jpcb.2c01288
J. Phys. Chem. B 2022, 126, 3897–3907

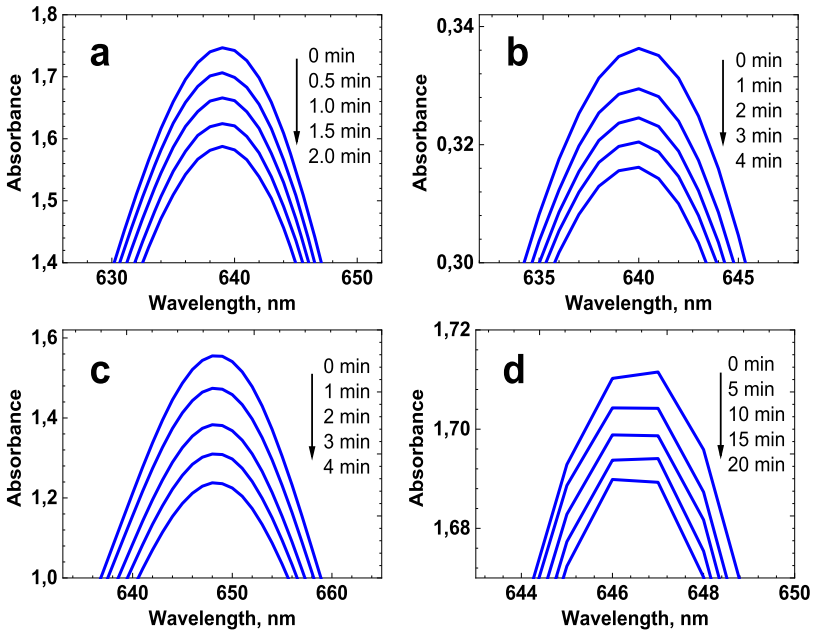

Figure 6. Photobleaching of the main linear absorption band of **1** (a,b) and **2** (c,d) in DCM (a,c) and TOL (b,d) under CW laser irradiation at 637 nm with beam irradiance ≈500 mW/cm^2. Corresponding irradiation times, t_{ir}, are indicated on the right.

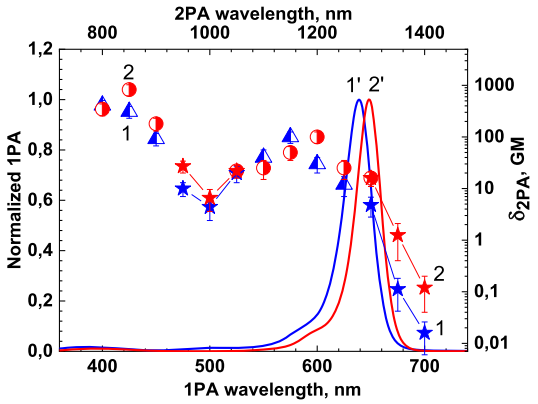

Figure 7. Degenerate 2PA (1, 2) and normalized linear 1PA spectra (1′, 2′, solid lines) of **1** (1, 1′) and **2** (2, 2′) in DCM. Circles are for **2** using Z-scan and triangles are for **1** using Z-scan. Stars show data (**1** blue, **2** red) obtained using the 2PF method. The 2PF data at 1050 nm and 1300 nm are calibrated using the Z-scan data at these wavelengths.

that two-photon transitions in the main linear absorption band are strictly forbidden for centrosymmetric molecules.[58] Nevertheless, the spectral position of the weak 2PA band roughly corresponded to the vibrational shoulder in the linear 1PA spectrum at ∼580 to 600 nm (Figure 7, curves 1′, 2′), and the nature of this band can be assigned to vibronic interactions with the asymmetric vibrational modes of **1** and **2**.[15,59] The shape of excitation anisotropy spectra (Figure 5, curves 1) revealed some higher excited electronic levels, S_n, in the spectral range 380−420 nm, which are in close proximity to the "double-resonance" excitation conditions for $S_0 \rightarrow S_n$ two-photon transitions,[35] and can explain a noticeable increase in the 2PA efficiency in this spectral range. In general, new squaraine **1** has 2PA properties similar to reference **2** and, according to a "figure of merit",[18] ($F_M = \delta_{2PA} \cdot \Phi_{fl}/\Phi_{ph} \approx 10^8$), exhibits high potential for application in two-photon fluorescence bioimaging.

The potential abilities of the squaraines **1** and **2** for light amplification were investigated in liquid solutions at room temperature under one-photon femtosecond transverse pumping in the main 1PA band with pump pulse energy $E_P \leq 5$ μJ (see Section 2.3). Efficient superluminescence emission was observed from relatively concentrated DCM solutions (C ∼ 10^{-4} M). Typical spectra are shown in Figure 8. The spontaneous fluorescence contours (Figure 8a,c, curves 4) were strongly reabsorbed under the employed concentrations and, consequently, transformed into much narrower superluminescence emission bands (curves 1, FWHM < 15 nm) with an increase in E_P. According to the data, the dependence of the collected emission intensity on the pump pulse energy revealed an obvious threshold character (Figure 8b,d) with the threshold values, $E_{th} \approx 0.12-0.15$ μJ, and exhibited linearity in the energy range $E_P < E_{th}$ (see insets in Figure 8b,d). It is worth mentioning that molecular superluminescence emission in bioimaging is a promising approach to expand modern laser scanning fluorescence microscopy methods.[18,19]

3.3. Theoretical Analysis of the Electronic Properties of 1 and 2. The nature of the electronic transitions in **1** and **2** was analyzed based on the DFT/TD-DFT theoretical approach using the Gaussian-2009 Rev.A02 suite of programs[49] and the PCM model[50] (see Section 2.4). Optimized molecular geometries in S_0 and S_1 electronic states, corresponding changes in the bond lengths under electronic excitation $S_0 \rightarrow S_1$, and the main calculated spectroscopic parameters of **1** and **2** in DCM are presented in Figure 9 and Table 2, respectively. All optimized geometries in Figure 9 revealed nearly planar molecular structures and the possibility of intramolecular hydrogen bonding between the hydroxyl groups and the oxygens of the squaric center. This is consistent with the experimentally observed high fluorescence quantum yields of **1** and **2** in DCM (see Table 1). The changes in the bond lengths under $S_0 \rightarrow S_1$ excitation were relatively small (≤0.013 Å) and nearly the same for **1** and **2**. Also, as deduced from the obtained data, the values of the calculated oscillator strengths and transition dipoles exhibit negligible dependence

https://doi.org/10.1021/acs.jpcb.2c01288
J. Phys. Chem. B 2022, 126, 3897−3907

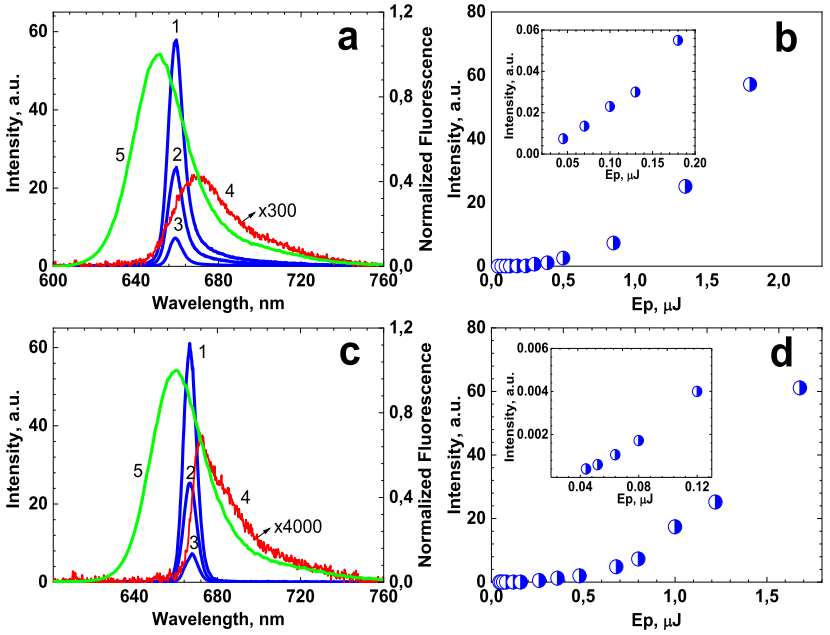

Figure 8. (a) Superluminescence bands of **1** in DCM at C ≈ $2 \cdot 10^{-4}$ M under femtosecond pumping with pulse energy E_P ≈ 1.8 μJ (1), 1.35 μJ (2), 0.85 μJ (3), 0.24 μJ (4), and normalized steady-state fluorescence spectrum of **1** in DCM at C ≈ $2 \cdot 10^{-7}$ M (5). (b) Dependence of collected emission intensity, I, on E_P for **1** in DCM at C ≈ $2 \cdot 10^{-4}$ M, and the corresponding initial part of this dependence (inset in (b)). (c) Superluminescence bands of **2** in DCM at C ≈ $3 \cdot 10^{-4}$ M under femtosecond pumping with E_P ≈ 1.68 μJ (1), 1.22 μJ (2), 0.8 μJ (3), 0.16 μJ (4), and normalized steady-state fluorescence spectrum of **2** in DCM at C ≈ 10^{-7} M (5). (d) Dependence $I = f(E_P)$ for **2** in DCM at C ≈ $3 \cdot 10^{-4}$ M, and the corresponding initial part of this dependence (inset in (d)).

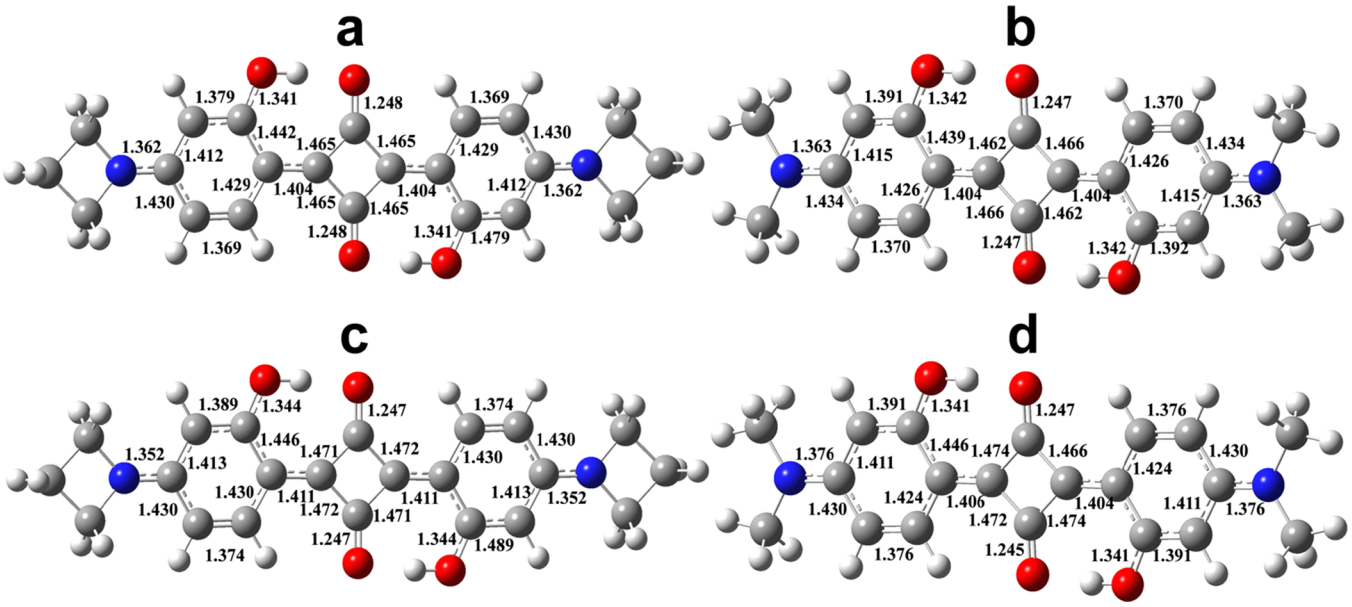

Figure 9. Optimized molecular geometries of **1** (a,c) and **2** (b,d) in DCM for S_0 (a,b) and S_1 (c,d) electronic states.

on the nature of the end substituents and do not explain the large difference in ε^{max} experimentally observed for **1** and **2** in DCM (i.e., ε^{max} (**1**) < ε^{max} (**2**). The absolute calculated value of the transition dipole μ_{01} for **2** in DCM is in a good agreement with the corresponding one estimated from the experimental spectral data (see Table 1). At the same time, even though solvent effects have been included, there is no perfect match of the calculated electronic transition wavelengths and experimental values of the absorption and emission maxima. Typical for the standard TD-DFT approach employed for cyanine dyes,[60] nevertheless, this method allows one to correctly analyze the nature of the first and several higher excited electronic states. Through comparison of the data in Figure 2 and Table 2, the main long-wavelength absorption bands of **1** and **2** correspond solely to the $S_0 \rightarrow S_1$ ($\pi \rightarrow \pi^*$) transition with nearly pure HOMO → LUMO configuration (HOMO and LUMO are the highest occupied and the lowest unoccupied molecular orbitals, respectively) and relatively high intensity (oscillator strength, $f \approx 1.75-1.94$). This is consistent with the experimentally observed constant values of anisotropy in the main 1PA bands of **1** and **2** (Figure 5, curves 1) and the large value of $\varepsilon^{max} \approx 4 \times 10^5$ M^{-1} cm^{-1} for reference squaraine

https://doi.org/10.1021/acs.jpcb.2c01288
J. Phys. Chem. B 2022, 126, 3897−3907

Table 2. Calculated Parameters of the Essential Excited States of 1 and 2: Wavelengths, λ, Oscillator Strength, f, Transition Dipoles μ_{01}, and Leading Configurations (HOMOs and LUMOs Are the Highest Occupied and the Lowest Unoccupied Molecular Orbitals, Respectively)

N/N	transition	λZ, nm	f	μ_{01}, Debye	type	main configurations
absorption of **1**	$S_0 \rightarrow S_1$	549.7	1.9402	15.04	$\pi \rightarrow \pi^*$	0.99| HOMO → LUMO>
	$S_0 \rightarrow S_2$	403.0	0.0000	0.00	$n \rightarrow \pi^*$	0.98| HOMO-4 → LUMO>
	$S_0 \rightarrow S_3$	402.8	0.0768	2.99	$\pi \rightarrow \pi^*$	0.97| HOMO-2 → LUMO>
	$S_0 \rightarrow S_4$	394.4	0.0000	0.00	$\pi \rightarrow \pi^*$	0.30| HOMO-3 → LUMO>
						−0.63| HOMO-1 → LUMO>
	$S_0 \rightarrow S_5$	350.6	0.0000	0.00	$\pi \rightarrow \pi^*$	0.61| HOMO-3 → LUMO>
						−0.27| HOMO-1 → LUMO>
fluorescence of **1**	$S_1 \rightarrow S_0$	560.4	1.8998		$\pi^* \rightarrow \pi$	0.71| LUMO → HOMO>
absorption of **2**	$S_0 \rightarrow S_1$	547.5	1.7882	14.42	$\pi \rightarrow \pi^*$	0.99| HOMO → LUMO>
	$S_0 \rightarrow S_2$	411.2	0.0000	0.00	$n \rightarrow \pi^*$	0.98| HOMO-4 → LUMO>
	$S_0 \rightarrow S_3$	410.7	0.0769	2.99	$\pi \rightarrow \pi^*$	0.45| HOMO-2 → LUMO>
						+0.49| HOMO-1 → LUMO>
	$S_0 \rightarrow S_4$	401.4	0.0000	0.00	$\pi \rightarrow \pi^*$	0.53| HOMO-2 → LUMO>
						−0.42| HOMO-1 → LUMO>
	$S_0 \rightarrow S_5$	354.8	0.0000	0.00	$\pi \rightarrow \pi^*$	0.63| HOMO-3 → LUMO>
fluorescence of **2**	$S_1 \rightarrow S_0$	556.8	1.7550		$\pi^* \rightarrow \pi$	0.71| LUMO →HOMO>

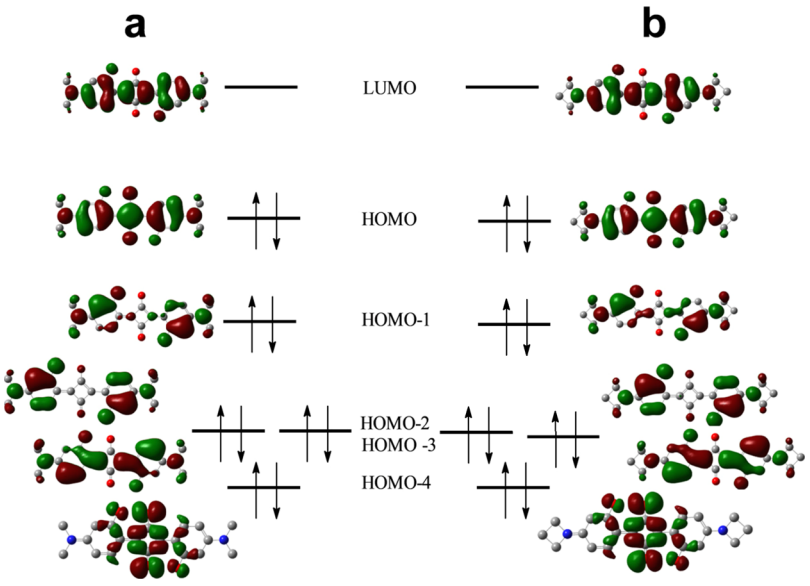

Figure 10. Main molecular orbitals of **1** (a) and **2** (b).

2. It is worth mentioning that the relatively small extinction coefficient $\varepsilon^{max} \approx 1.35 \times 10^5$ M^{-1} cm^{-1} for new squaraine **1** is not explained by the employed theoretical approach. As follows from the data in Table 2, calculated transitions into the higher excited electronic states $S_0 \rightarrow S_n$ (n = 2−5) exhibit weak intensity (f < 0.08), and the different nature depends on the participating molecular orbitals. This prediction is in good agreement with the very weak absorption in the short wavelength range of the experimental 1PA spectra of **1** and **2** (Figure 2, curves 1). The main frontier molecular orbitals of **1** and **2** (Figure 10) participating in the first 5 electronic transitions belong to HOMO type and only one to the LUMO type that is typical of symmetrical squaraines in the red-NIR spectral range.[17,18] As follows from the data in Table 2 and Figure 10, there is only one $n \rightarrow \pi^*$ electron transition ($S_0 \rightarrow S_2$), which involves a lone electron pair at the corresponding oxygen atoms and exhibits negligible transition dipole moment. In general, the nature of the main electronic transitions of **1** and **2** are similar to each other and mostly correspond to experimental results along with other calculated parameters.

4. CONCLUSIONS

A comprehensive investigation of the linear photophysical, 2PA, suplerluminescence, and photochemical properties of new symmetrical squaraine derivative **1** was performed in liquid solutions at room temperature along with the quantum chemical analysis. Steady-state absorption, fluorescence, and fundamental excitation anisotropy spectra of **1** revealed relatively narrow absorption and emission bands (FWHM ≈ 30 nm), small Stokes shifts (<15 nm), high quantum yields ($\Phi_{fl} \approx 0.8-1.0$), only one electronic transition $S_0 \rightarrow S_1$ in the main long-wavelength absorption band, and an angle of ≈25° between the absorption, $\boldsymbol{\mu}_{01}$, and emission, $\boldsymbol{\mu}_{10}$, transition dipoles. All these parameters are similar to known reference squaraine **2** (and typical for other symmetric squaraines in the red-NIR spectral range[18,27]), except for the value of the maximum extinction coefficient $\varepsilon^{max} \approx 1.35 \times 10^5$ M^{-1} cm^{-1}.

https://doi.org/10.1021/acs.jpcb.2c01288
J. Phys. Chem. B 2022, 126, 3897−3907

This value is noticeably smaller than that expected from the linear steady-state and time-resolved spectral data and theoretical prediction, and the origin remains unclear. The degenerate 2PA spectrum of **1** was obtained over a broad spectral range and a maximum cross-section of $\delta_{2PA}^{max} \approx 400$ GM was shown at ~800 nm, where the double-resonance excitation conditions can be expected.

The phenomenon of superluminescence emission was observed for **1** and **2** in polar DCM at room temperature under 1 kHz femtosecond pumping with a corresponding threshold energy ~0.12 to 0.15 μJ and is potentially important for the development of spectrally bright fluorescence labels for bioimaging. The results of DFT/TD-DFT based quantum-chemical calculations were in good agreement with the main spectroscopic parameters of **1** and revealed the nature of the main 1PA band. Linear photophysical properties, 2PA efficiency, superluminescence phenomenon in the red-NIR spectral range, and high photostability of azetidyl squaraine **1** suggest that it has promising potential for two-photon fluorescence bioimaging applications.

AUTHOR INFORMATION

Corresponding Authors

Mykhailo V. Bondar − *CREOL, The College of Optics and Photonics, University of Central Florida, Orlando, Florida 32816, United States; Institute of Physics NASU, Kyiv-28 03028, Ukraine*; Email: Mykhailo.Bondar@ucf.edu

David J. Hagan − *CREOL, The College of Optics and Photonics, University of Central Florida, Orlando, Florida 32816, United States;* orcid.org/0000-0003-2713-1767; Email: hagan@creol.ucf.edu

Authors

Sanaz Faryadras − *CREOL, The College of Optics and Photonics, University of Central Florida, Orlando, Florida 32816, United States*

Natalia Munera − *CREOL, The College of Optics and Photonics, University of Central Florida, Orlando, Florida 32816, United States*

Hao-Jung Chang − *CREOL, The College of Optics and Photonics, University of Central Florida, Orlando, Florida 32816, United States;* orcid.org/0000-0002-4207-1056

Mehrun Uddin − *Department of Chemistry and Environmental Science, College of Science and Liberal Arts, New Jersey Institute of Technology, University Heights, Newark, New Jersey 07102, United States*

Kevin D. Belfield − *Department of Chemistry and Environmental Science, College of Science and Liberal Arts, New Jersey Institute of Technology, University Heights, Newark, New Jersey 07102, United States;* orcid.org/0000-0002-7339-2813

Olexiy D. Kachkovsky − *V.P. Kukhar Institute of Bioorganic Chemistry and Petrochemistry, Kyiv 02660, Ukraine*

Eric W. Van Stryland − *CREOL, The College of Optics and Photonics, University of Central Florida, Orlando, Florida 32816, United States*

Complete contact information is available at: https://pubs.acs.org/10.1021/acs.jpcb.2c01288

Notes

The authors declare no competing financial interest.

ACKNOWLEDGMENTS

M.V.B. wishes to thank the National Academy of Sciences of Ukraine (B/204). E.V.S., H.J.C., and D.J.H. thank the National Science Foundation grant DMR-1609895 for support. K.D.B. wishes to acknowledge support from the National Science Foundation (CBET-1517273 and CHE-1726345) and the National Institutes of Health (R21AA028340).

REFERENCES

(1) (a) Prabhakar, C.; Bhanuprakash, K.; Rao, V. J.; Balamuralikrishna, M.; Narayana Rao, D. Third order nonlinear optical properties of squaraine dyes having absorption below 500 nm: A combined experimental and theoretical investigation of closed shell oxyallyl derivatives. *J. Phys. Chem. C* **2010**, *114*, 6077−6089. (b) Webster, S.; Fu, J.; Padilha, L. A.; Przhonska, O. V.; Hagan, D. J.; Van Stryland, E. W.; Bondar, M. V.; Slominsky, Y. L.; Kachkovski, A. D. Comparison of nonlinear absorption in three similar dyes: Polymethine, squaraine and tetraone. *Chem. Phys.* **2008**, *348*, 143−151. (c) Chung, S.-J.; Zheng, S.; Odani, T.; Beverina, L.; Fu, J.; Padilha, L. A.; Biesso, A.; Hales, J. M.; Zhan, X.; Schmidt, K.; et al. Extended squaraine dyes with large two-photon absorption cross-sections. *J. Am. Chem. Soc.* **2006**, *128*, 14444−14445. (d) Chen, C.-T.; Marder, S. R.; Cheng, L.-T. Syntheses and linear and nonlinear optical properties of unsymmetrical squaraines with extended conjugation. *J. Am. Chem. Soc.* **1994**, *116*, 3117−3118.

(2) (a) Jipson, V. B.; Jones, C. R. Infrared dyes for optical storage. *J. Vac. Sci. Technol.* **1981**, *18*, 105−109. (b) Emmelius, M.; Pawlowski, G.; Vollmann, H. W. Materials for optical data storage. *Angew. Chem., Int. Ed.* **1989**, *28*, 1445−1471. (c) Rong, A.; Huang, D.; Chen, Q. Ultrahigh density recording based on third-order optical non-linearities. *Proc. SPIE* **2001**, *4085*, 208−215.

(3) (a) Kim, J. H.; Liess, A.; Stolte, M.; Krause, A.-M.; Stepanenko, V.; Zhong, C.; Bialas, D.; Spano, F.; Würthner, F. An efficient narrowband near-infrared at 1040 nm organic photodetector realized by intermolecular charge transfer mediated coupling based on a squaraine dye. *Adv. Mater.* **2021**, *33*, No. 2100582. (b) Paterno, G. M.; Barbero, N.; Galliano, S.; Barolo, C.; Lanzani, G.; Scotognella, F.; Borrelli, R. Excited state photophysics of squaraine dyes for photovoltaic applications: an alternative deactivation scenario. *J. Mater. Chem. C* **2018**, *6*, 2778−2785. (c) Schulz, M.; Mack, M.; Kolloge, O.; Lutzena, A.; Schiek, M. Organic photodiodes from homochiral L-proline derived squaraine compounds with strong circular dichroism. *Phys. Chem. Chem. Phys.* **2017**, *19*, 6996−7008. (d) Maeda, T.; Nitta, S.; Nakao, H.; Yagi, S.; Nakazumi, H. Squaraine dyes with pyrylium and thiopyrylium components for harvest of near infrared light in dye sensitized solar cells. *J. Phys. Chem. C* **2014**, *118*, 16618−16625.

(4) He, J.; Jo, Y. J.; Sun, X.; Qiao, W.; Ok, J.; Kim, T.-i.; Li, Z. Squaraine dyes for photovoltaic and biomedical applications. *Adv. Funct. Mater.* **2021**, *31*, No. 2008201.

(5) Chen, Y.; Wang, G.; Yang, L.; Wu, J.; Melkonyan, F. S.; Huang, Y.; Lu, Z.; Marks, T. J.; Facchetti, A. Novel unsymmetrical squaraine-based small molecules for organic solar cells. *J. Mater. Chem. C* **2018**, *6*, 847−854.

(6) (a) Wang, G.; Chen, H.; Chen, Y.; Fu, N. A near-infrared squaraine dye for cascade recognition of copper ion and biological phosphate and its application in IMPLICATION logic gate. *Sens. Actuators, B* **2016**, *233*, 550−558. (b) Wang, Y.; Wang, C.; Xue, S.; Liang, Q.; Li, Z.; Xu, S. Highly selective and sensitive colorimetric and fluorescent chemosensor of Fe^{3+} and Cu^{2+} based on 2,3,3-trimethylnaphto[1,2-*d*] squaraine. *RSC Adv.* **2016**, *6*, 6540−6550. (c) Sun, J.; Ye, B.; Xia, G.; Wang, H. A multi-responsive squaraine-based "turn on" fluorescent chemosensor for highly sensitive detection of Al^{3+}, Zn^{2+} and Cd^{2+} in aqueous media and its biological application. *Sens. Actuators, B* **2017**, *249*, 386−394. (d) Philips, D. S.; Ghosh, S.; Sudheesh, K. V.; Suresh, C. H.; Ajayaghosh, A. An unsymmetrical squaraine-dye-based chemical platform for multiple analyte recognition. *Chem. − Eur. J.* **2017**, *23*, 17973−17980. (e) Zhu,

H.; Fan, J.; Chen, H.; Tang, Z.; Wang, G.; Fu, N. An EDTA promoted coordination induced disaggregation for specific Hg^{2+} detection. *Dyes Pigm.* **2015**, *113*, 181−188.
(7) (a) Butnarasu, C.; Barbero, N.; Viscardi, G.; Visentin, S. Unveiling the interaction between PDT active squaraines with ctDNA: A spectroscopic study. *Spectrochim. Acta, Part A* **2021**, *250*, No. 119224. (b) Babu, P. S.; Manu, P. M.; Dhanya, T. J.; Tapas, P.; Meera, R. N.; Surendran, A.; Aneesh, K. A.; Vadakkancheril, S. J.; Ramaiah, D.; Nair, S. A.; et al. Bis(3,5-diiodo-2,4,6-trihydroxyphenyl)-squaraine photodynamic therapy disrupts redox homeostasis and induce mitochondria-mediated apoptosis in human breast cancer cells. *Sci. Rep.* **2017**, *7*, 42126. (c) Miletto, I.; Fraccarollo, A.; Barbero, N.; Barolo, C.; Cossi, M.; Marchese, L.; Gianotti, E. Mesoporous silica nanoparticles incorporating squaraine-based photosensitizers: a combined experimental and computational approach. *Dalton Trans.* **2018**, *47*, 3038−3046. (d) Abrahamse, H.; Hamblin, M. R. New photosensitizers for photodynamic therapy. *Biochem. J.* **2016**, *473*, 347−364.
(8) Avirah, R. R.; Jayaram, D. T.; Adarsh, N.; Ramaiah, D. Squaraine dyes in PDT: from basic design to in vivo demonstration. *Org. Biomol. Chem.* **2012**, *10*, 911−920.
(9) Yi, R.; Das, P.; Lin, F.; Shen, B.; Yang, Z.; Zhao, Y.; Hong, L.; He, Y.; Hu, R.; Song, J.; et al. Fluorescence enhancement of small squaraine dye and its two-photon excited fluorescence in long-term near-infrared I&II bioimaging. *Opt. Express* **2019**, *27*, 12360−12372.
(10) (a) Jiang, X.; Rong, L.; Cao, J.; Fu, N. Near-infrared fluorescent probe for tracing diquat in aqueous solutions and bioimaging in *vivo*. *Dyes Pigm.* **2021**, *191*, No. 109375. (b) Shaw, S. K.; Liu, W.; Brennan, S. P.; Betancourt-Mendiola, M. L.; Smith, B. D. Non-covalent assembly method that simultaneously endows a liposome surface with targeting ligands, protective PEG chains, and deep-red fluorescence reporter groups. *Chem. − Eur. J.* **2017**, *23*, 12646−12654. (c) Peck, E. M.; Battles, P. M.; Rice, D. R.; Roland, F. M.; Norquest, K. A.; Smith, B. D. Pre-assembly of near-infrared fluorescent multivalent molecular probes for biological imaging. *Bioconjugate Chem.* **2016**, *27*, 1400−1410. (d) Cole, E. L.; Arunkumar, E.; Xiao, S.; Smith, B. A.; Smith, B. D. Water-soluble, deep-red fluorescent squaraine rotaxanes. *Org. Biomol. Chem.* **2012**, *10*, 5769−5773.
(11) Sun, C.-L.; Lv, S.-K.; Liu, Y.-P.; Liao, Q.; Zhang, H.-L.; Fu, H.; Yao, J. Benzoindolic squaraine dyes with a large two-photon absorption cross-section. *J. Mater. Chem. C* **2017**, *5*, 1224−1230.
(12) Sreejith, S.; Carol, P.; Chithra, P.; Ajayaghosh, A. Squaraine dyes: a mine of molecular materials. *J. Mater. Chem.* **2008**, *18*, 264−274.
(13) Qiao, W.; Yao, P.; Chen, Y.; Xiao, Q.; Zhang, L.; Li, Z. Squaraine-based AIEgens for reversible mechanochromism, sensitive and selective hypochlorite detection and photostable far-red fluorescence cell imaging. *Mater. Chem. Front.* **2020**, *4*, 2688−2696.
(14) Odom, S. A.; Webster, S.; Padilha, L. A.; Peceli, D.; Hu, H.; Nootz, G.; Chung, S. J.; Ohira, S.; Matichak, J. D.; Przhonska, O. V.; et al. Synthesis and two-photon spectrum of a bis(porphyrin)-substituted squaraine. *J. Am. Chem. Soc.* **2009**, *131*, 7510−7511.
(15) Scherer, D.; Dorfler, R.; Feldner, A.; Vogtmann, T.; Schwoerer, M.; Lawrentz, U.; Grahn, W.; Lambert, C. Two-photon states in squaraine monomers and oligomers. *Chem. Phys.* **2002**, *279*, 179−207.
(16) Kaczmarek-Kędziera, A.; Kędziera, D. Computational study of the influence of nitrogen-containing unsaturated heterocyclic substituents on electronic and spectroscopic properties of squaraine derivatives. *J. Phys. Chem. A* **2019**, *123*, 2387−2400.
(17) Chang, H.-J.; Bondar, M. V.; Liu, T.; Liu, X.; Singh, S.; Belfield, K. D.; Sheely, A.; Masunov, A. E.; Hagan, D. J.; Van Stryland, E. W. Electronic nature of neutral and charged two-photon absorbing squaraines for fluorescence bioimaging application. *ACS Omega* **2019**, *4*, 14669−14679.
(18) Belfield, K. D.; Bondar, M. V.; Haniff, H. S.; Mikhailov, I. A.; Luchita, G.; Przhonska, O. V. Superfluorescent squaraine with efficient two-photon absorption and high photostability. *ChemPhysChem* **2013**, *14*, 3532−3542.
(19) Liu, T.; Bondar, M. V.; Belfield, K. D.; Anderson, D.; Masunov, A. E.; Hagan, D. J.; Van Stryland, E. W. Linear photophysics and femtosecond nonlinear spectroscopy of a star-shaped squaraine derivative with efficient two-photon absorption. *J. Phys. Chem. C* **2016**, *120*, 11099−11110.
(20) Wang, S.; Hall, L.; Diev, V. V.; Haiges, R.; Wei, G.; Xiao, X.; Djurovich, P. I.; Forrest, S. R.; Thompson, M. E. N,N-diarylanilinosquaraines and their application to organic photovoltaics. *Chem. Mater.* **2011**, *23*, 4789−4798.
(21) Chua, M. H.; Zhou, H.; Lin, T. T.; Wu, J.; Xu, J. Triphenylethylene- and tetraphenylethylene-functionalized 1,3-bis-(pyrrol-2-yl)squaraine dyes: ynthesis, aggregation-caused quenching to aggregation-induced emission, and thiol detection. *ACS Omega* **2018**, *3*, 16424−16435.
(22) (a) Liu, T.; Liu, X.; Wang, W.; Luo, Z.; Liu, M.; Zou, S.; Sissa, C.; Painelli, A.; Zhang, Y.; Vengris, M.; et al. Systematic molecular engineering of a series of aniline-based squaraine dyes and their structure-related properties. *J. Phys. Chem. C* **2018**, *122*, 3994−4008. (b) Wu, J.; Si, C.; Chen, Y.; Yang, L.; Hu, B.; Chen, G.; Lu, Z.; Huang, Y. Photovoltaic devices prepared through a trihydroxy substitution strategy on an unsymmetrical squaraine dye. *Chem. − Eur. J.* **2018**, *24*, 3234−3240.
(23) Paek, S.; Choi, H.; Kim, C.; Cho, N.; So, S.; Song, K.; Nazeeruddinc, M. K.; Ko, J. Efficient and stable panchromatic squaraine dyes for dye-sensitized solar cells. *Chem. Commun.* **2011**, *47*, 2874−2876.
(24) Pisoni, D. d. S.; Petzhold, C. L.; de Abreu, M. P.; Rodembusch, F. S.; Campo, L. F. Synthesis, spectroscopic characterization and photophysical study of dicyanomethylene substituted squaraine dyes. *C. R. Chim.* **2012**, *15*, 454−462.
(25) Hu, L.; Yan, Z.; Xu, H. Advances in synthesis and application of near-infrared absorbing squaraine dyes. *RSC Adv.* **2013**, *3*, 7667−7676.
(26) Somashekharappa, G. M.; Govind, C.; Pulikodan, V.; Paul, M.; Namboothiry, M. A. G.; Das, S.; Karunakaran, V. Unsymmetrical squaraine dye-based organic photodetector exhibiting enhanced near-infrared sensitivity. *J. Phys. Chem. C* **2020**, *124*, 21730−21739.
(27) Chen, G.; Sasabe, H.; Sasaki, Y. Z.; Katagiri, H.; Wang, X.-F.; Sano, T.; Hong, Z.; Yang, Y.; Kido, J. A series of squaraine dyes: Effects of side chain and the number of hydroxyl groups on material properties and photovoltaic performance. *Chem. Mater.* **2014**, *26*, 1356−1364.
(28) (a) Bassal, F.; Laurent, A. D.; Le Guennic, B.; Jacquemin, D. Exploring the excited-states of squaraine dyes with TD-DFT, SOS-CIS(D) and ADC(2). *Dyes Pigm.* **2017**, *138*, 169−175. (b) Maltese, V.; Cospito, S.; Beneduci, A.; De Simone, B. C.; Russo, N.; Chidichimo, G.; Janssen, R. A. J. Electro-optical properties of neutral and radical ion thienosquaraines. *Chem. − Eur. J.* **2016**, *22*, 10179−10186.
(29) Alberto, G.; Barbero, N.; Divieto, C.; Rebba, E.; Sassi, M. P.; Viscardi, G.; Martra, G. Solid silica nanoparticles as carriers of fluorescent squaraine dyes in aqueous media: Toward a molecular engineering approach. *Colloids Surf., A* **2019**, *568*, 123−130.
(30) Wickramsinghe, P.; Deokar, P.; Djurovich, P. I.; Haiges, R.; Thompson, M. E. Symmetric pyrrolic squaraines and their application to organic photovoltaics. *J. Photochem. Photobiol., A* **2019**, *374*, 16−21.
(31) Cornelissen-Gude, C.; Rettig, W.; Lapouyade, R. Photophysical properties of squaraine derivatives: evidence for charge separation. *J. Phys. Chem. A* **1997**, *101*, 9673−9677.
(32) Webster, S.; Peceli, D.; Hu, H.; Padilha, L. A.; Przhonska, O. V.; Masunov, A. E.; Gerasov, A. O.; Kachkovski, A. D.; Slominsky, Y. L.; Tolmachev, A. I.; et al. Near-unity quantum yields for intersystem crossing and singlet oxygen generation in polymethine-like molecules: Design and experimental realization. *J. Phys. Chem. Lett.* **2010**, *1*, 2354−2360.
(33) Ballestas-Barrientos, A. R.; Woodward, A. W.; Moreshead, W. V.; Bondar, M. V.; Belfield, K. D. Synthesis and linear and nonlinear

https://doi.org/10.1021/acs.jpcb.2c01288
J. Phys. Chem. B 2022, 126, 3897−3907

photophysical characterization of two symmetrical pyrene-terminated squaraine derivatives. *J. Phys. Chem. C* **2016**, *120*, 7829−7838.
(34) Toro, C.; De Boni, L.; Yao, S.; Ritchie, J. P.; Masunov, A. E.; Belfield, K. D.; Hernandez, F. E. Linear and nonlinear optical characterizations of a monomeric symmetric squaraine-based dye in solution. *J. Chem. Phys.* **2009**, *130*, 214504.
(35) Fu, J.; Padilha, L. A.; Hagan, D. J.; Van Stryland, E. W.; Przhonska, O. V.; Bondar, M. V.; Slominsky, Y. L.; Kachkovski, A. D. Experimental and theoretical approaches to understanding two-photon absorption spectra in polymethine and squaraine molecules. *J. Opt. Soc. Am. B* **2007**, *24*, 67−76.
(36) (a) Beverina, L.; Salice, P. Squaraine compounds: Tailored design and synthesis towards a variety of material science applications. *Eur. J. Org. Chem.* **2010**, *2010*, 1207−1225. (b) Langmar, O.; Saccone, D.; Amat, A.; Fantacci, S.; Viscardi, G.; Barolo, C.; Costa, R. D.; Guldi, D. M. Designing squaraines to control charge injection and recombination processes in NiO-based dye-sensitized solar cells. *ChemSusChem* **2017**, *10*, 2385−2393. (c) Xiao, Q.; Yang, S.; Wang, R.; Zhang, Y.; Zhang, H.; Zhou, H.; Li, Z. Synthesis, structure and material properties of thiopyranylidene-based asymmetrical squaraines. *Dyes Pigm.* **2018**, *154*, 137−144.
(37) (a) Bonomo, M.; Magistris, C.; Buscaino, R.; Fin, A.; Barolo, C.; Dini, D. Effect of sodium hydroxide pretreatment of NiO_x cathodes on the performance of squaraine-sensitized *p*-type dye-sensitized solar cells. *ChemistrySelect* **2018**, *3*, 1066−1075. (b) Geiger, T.; Kuster, S.; Yum, J.-H.; Moon, S.-J.; Nazeeruddin, M. K.; Gratzel, M.; Nuesch, F. Molecular design of unsymmetrical squaraine dyes for high efficiency conversion of low energy photons into electrons using TiO_2 nanocrystalline films. *Adv. Funct. Mater.* **2009**, *19*, 2720−2727. (c) Alagumalai, A.; Fairoos, M. K. M.; Vellimalai, P.; Sil, M. C.; Nithyanandhan, J. Effect of out-of-plane alkyl group's position in dye-sensitized solar cell efficiency: A structure-property relationship utilizing indoline-based unsymmetrical squaraine dyes. *ACS Appl. Mater. Interfaces* **2016**, *8*, 35353−35367.
(38) (a) Ahn, H.-Y.; Yao, S.; Wang, X.; Belfield, K. D. Near-infrared-emitting squaraine dyes with high 2PA cross-sections for multiphoton fluorescence imaging. *ASC Appl. Mater. Interfaces* **2012**, *4*, 2847−2854. (b) Karpenko, I. A.; Klymchenko, A. S.; Gioria, S. P.; Kreder, R.; Shulov, I.; Villa, P.; Mely, Y.; Hibert, M.; Bonnet, D. Squaraine as a bright, stable and environment sensitive far-red label for receptor-specific cellular imaging. *Chem. Commun.* **2015**, *51*, 2960−2963. (c) Kabatc, J.; Kostrzewska, K.; Jurek, K.; Dobosz, R.; Orzeł, L. 1,3-bis(phenylamino)squaraine - Photophysical and photochemical properties. *Dyes Pigm.* **2016**, *127*, 179−186.
(39) Qaddoura, M. A.; Belfield, K. D.; Tongwa, P.; DeSanto, J. E.; Timofeeva, T. V.; Heiney, P. A. Thermotropic behaviour, self-assembly and photophysical properties of a series of squaraines. *Supramol. Chem.* **2011**, *23*, 731−742.
(40) Grimm, J.; English, B.; Chen, J.; Slaughter, J. P.; Zhang, Z.; Revyakin, A.; Patel, R.; Macklin, J. J.; Normanno, D.; Singer, R. H.; et al. A general method to improve fluorophores for live-cell and single-molecule microscopy. *Nat. Methods* **2015**, *12*, 244−250.
(41) Kazmaier, P. M.; Hamer, G. K.; Burt, R. A. Conformational isomerism in squaraines: saturation transfer NMR studies on hydroxy squaraines. *Can. J. Chem.* **1990**, *68*, 530−536.
(42) Lakowicz, J. R. *Principles of fluorescence spectroscopy*; Kluwer, 1999.
(43) Magde, D.; Brannon, J. H.; Cremers, T. L.; Olmsted, J., III Absolute luminescence yield of Cresyl Violet. A standard for the red. *J. Phys. Chem.* **1979**, *83*, 696−699.
(44) Arrhenius, S. The relaxation time and dipole moment of Gliadin. *J. Chem. Phys.* **1937**, *5*, 63−66.
(45) Corredor, C. C.; Belfield, K. D.; Bondar, M. V.; Przhonska, O. V.; Yao, S. One- and two-photon photochemical stability of linear and branched fluorene derivatives. *J. Photochem. Photobiol., A* **2006**, *184*, 105−112.
(46) (a) Zhao, P.; Tofighi, S.; O'Donnell, R. M.; Shi, J.; Zavalij, P. Y.; Bondar, M. V.; Hagan, D. J.; Van Stryland, E. W. Electronic nature of new Ir(III)-complexes: Linear spectroscopic and nonlinear optical properties. *J. Phys. Chem. C* **2017**, *121*, 23609−23617. (b) Zhao, P.; Tofighi, S.; O'Donnell, R. M.; Shi, J.; Bondar, M. V.; Hagan, D. J.; Van Stryland, E. W. Dual emissive multinuclear Iridium(III) complexes in solutions: Linear photophysical properties, two- photon absorption spectra, and photostability. *J. Phys. Chem. C* **2018**, *122*, 6786−6793.
(47) Sheik-Bahae, M.; Said, A. A.; Wei, T. H.; Hagan, D. J.; Van Stryland, E. W. Sensitive measurement of optical nonlinearities using a single beam. *IEEE J. Quantum Electron.* **1990**, *26*, 760−769.
(48) Xu, C.; Webb, W. W. Measurement of two-photon excitation cross sections of molecular fluorophores with data from 690 to 1050 nm. *J. Opt. Soc. Am. B* **1996**, *13*, 481−491.
(49) *Gaussian 09, Revision A.2*; Gaussian, Inc.: Wallingford CT, 2009. (accessed).
(50) Tomasi, J.; Mennucci, B.; Cammi, R. Quantum mechanical continuum solvation models. *Chem. Rev.* **2005**, *105*, 2999−3094.
(51) (a) Dirk, C. W.; Herndon, W. C.; Cervantes-Lee, F.; Selnau, H.; Martinez, S.; Kalamegham, P.; Tan, A.; Campos, G.; Velez, M.; Zyss, J.; et al. Squarylium dyes: Structural factors pertaining to the negative third-order nonlinear optical response. *J. Am. Chem. Soc.* **1995**, *117*, 2214−2225. (b) Tong, L.; Bixian, P. The Influence of *n*-alkyl groups on the properties of squarylium cyanine dyes. *Dyes Pigm.* **1998**, *39*, 201−209.
(52) Hales, J. M.; Matichak, J.; Barlow, S.; Ohira, S.; Yesudas, K.; Brédas, J.-L.; Perry, J. W.; Marder, S. R. Design of polymethine dyes with large third-order optical nonlinearities and loss figures of merit. *Science* **2010**, *327*, 1485−1488.
(53) Strickler, S. J.; Berg, R. A. Relationship between absorption intensity and fluorescence lifetime of molecules. *J. Chem. Phys.* **1962**, *37*, 814−822.
(54) Birks, J. B.; Dyson, D. J. The relations between the fluorescence and absorption properties of organic molecules. *Proc. R. Soc. London, Ser. A* **1963**, *275*, 135−148.
(55) Belfield, K. D.; Bondar, M. V.; Hales, J. M.; Morales, A. R.; Przhonska, O. V.; Schafer, K. J. One- and two-photon fluorescence anisotropy of selected fluorene derivatives. *J. Fluoresc.* **2005**, *15*, 3−11.
(56) Ollis, D.; Mills, A.; Lawrie, K. Kinetics of methylene blue (MB) photocatalyzed reduction and dark regeneration in a colorimetric oxygen sensor. *Appl. Catal., B* **2016**, *184*, 201−207.
(57) (a) El-Daly, S. A.; El-Azim, S. A.; Elmekawey, F. M.; Elbaradei, B. Y.; Shama, S. A.; Asiri, A. M. Photophysical parameters, excitation energy transfer, and photoreactivity of 1,4-bis(5-phenyl-2-oxazolyl)-benzene (POPOP) laser dye. *Int. J. Photoenergy* **2012**, *2012*, No. 458126. (b) Azim, S. A.; Al-Hazmy, S. M.; Ebeid, E. M.; El-Daly, S. A. A new coumarin laser dye 3-(benzothiazol-2-yl)-7-hydroxycoumarin. *Opt. Laser Technol.* **2005**, *37*, 245−249.
(58) Peticolas, W. L. Multiphoton spectroscopy. *Ann. Rev. Phys. Chem.* **1967**, *18*, 233−260.
(59) Fu, J.; Przhonska, O. V.; Padilha, L. A.; Hagan, D. J.; Van Stryland, E. W.; Belfield, K. D.; Bondar, M. V.; Slominsky, Y. L.; Kachkovski, A. D. Two-photon anisotropy: analytical description and molecular modeling for symmetrical and asymmetrical organic dyes. *Chem. Phys.* **2006**, *321*, 257−268.
(60) Fabian, J. TDDFT-calculations of Vis/NIR absorbing compounds. *Dyes Pigm.* **2010**, *84*, 36−53. Karaca, S.; Elmacı, N. A computational study on the excited state properties of a cationic cyanine dye: TTBC. *Comput. Theor. Chem.* **2011**, *964*, 160−168.

https://doi.org/10.1021/acs.jpcb.2c01288
J. Phys. Chem. B 2022, 126, 3897−3907